PCCP

ROYAL SOCIETY OF CHEMISTRY

PAPER

View Article Online
View Journal | View Issue

Cite this: *Phys. Chem. Chem. Phys.*, 2023, **25**, 12342

Restriction of crossing conical intersections: the intrinsic mechanism of aggregation-induced emission†

Jie Peng,‡[ab] Xin He,‡[a] Yao Li,[b] Jianxin Guan,[a] Baihua Wu,[a] Xinmao Li,[a] Zhihao Yu,[a] Jian Liu *[a] and Junrong Zheng *[a]

Received 9th November 2022,
Accepted 28th March 2023

DOI: 10.1039/d2cp05256c

rsc.li/pccp

Elucidating the mechanism of aggregation-induced emission (AIE) is a prerequisite for designing more AIE-gens. The diphenylethylene (DPE) featured molecules are one of the most important AIE-gens due to their propeller structure. Three representative DPE-featured AIE-gens, triphenylethylene, *cis*-stilbene, and *trans*-stilbene, are explored *via* ultrafast ultraviolet/infrared (UV/IR) spectroscopy and theoretical calculations. Both experimental and computational results suggest that readily crossing conical intersections (CIs) with flexible structural evolutions in solutions significantly reduces fluorescence, whereas crossing CIs is restricted because of high energy cost, and therefore no fast nonradiative decay can compete with spontaneous emission in solids. The mechanism also well explains the different emission quantum yields and interconversion ratios between *cis*-stilbene and *trans*-stilbene after photoexcitation.

I. Introduction

Organic light-emitting materials are of great significance for both practical applications and fundamental research.[1–4] Most luminescent materials that have been widely reported are either aggregation-caused quenching (ACQ) or aggregation-induced emission (AIE) fluorophores. For ACQ molecules, although their emission is strong in dilute solutions, they often suffer from quenching when their concentrations are increased.[5] In contrast, materials with the aggregation-induced emission (AIE) feature emit weakly in solution, but strongly in the aggregated state,[6–10] which has been well documented in the literature for more than 100 years.[11–13] Nevertheless, AIE was first named in 2001[6] and received widespread attention afterward. Most AIE fluorophores have a propeller structure, among which the diphenylethylene (DPE) fragments often appear, such as in hexaphenylsilole (HPS), tetraphenylethene (TPE) and their derivatives.[6,14–16]

Many AIE-gens have been discovered and synthesized in the past two decades, but the mechanism of AIE has not been fully understood. In the early days, it was generally accepted that the restriction of intramolecular vibration and rotation (RIV and RIR) was the reason for the recovery of fluorescence in solids.[14,17–20] This mechanism is intuitively reasonable and widely cited, but it does not provide detailed information about how electronic excitation is nonradiatively converted into thermal energy. In recent years, mechanistic studies have revealed more quantitative details about AIE. As for AIE-gens with the DPE fragment, computational results suggest that the excited fluorophores in solution pass through a conical intersection (CI),[21,22] either *via* photocyclization[23–25] or *E*/*Z* isomerization[26–29] (Scheme 1) and dissipate the electronically excited energy *via* nonradiative decay at the CI configuration.

However, crossing CIs is mainly concluded as the major reason for the weak luminescence of AIE solutions based on theoretical calculations but it lacks experimental evidence.[25,30,31] In previous work, we reported the direct observation of cyclic intermediates of photoexcited TPE and its derivatives in solutions *via* ultraviolet/infrared (UV/IR) mixed frequency ultrafast spectroscopy.[32,33] The work provides experimental evidence to support that photocyclization by crossing CIs in solutions results in an efficient nonradiative decay to suppress fluorescence, whereas the inaccessibility of CIs besides the considerable separation of chromophores in solids helps retain the spontaneous emission. The mechanism works well for the studied AIE molecules,[32,33] but whether it is general for other AIE systems remains to be answered. Herein, three molecules with the DPE segment, triphenylethylene, *cis*-stilbene, and *trans*-stilbene, are

[a] College of Chemistry and Molecular Engineering, Beijing National Laboratory for Molecular Sciences, Peking University, Beijing 100871, China. E-mail: junrong@pku.edu.cn, jianliupku@pku.edu.cn
[b] Sinopec Nanjing Research Institute of Chemical Industry Co., Ltd, Nanjing 210048, China

† Electronic supplementary information (ESI) available. See DOI: https://doi.org/10.1039/d2cp05256c

‡ These authors contributed equally to this work.

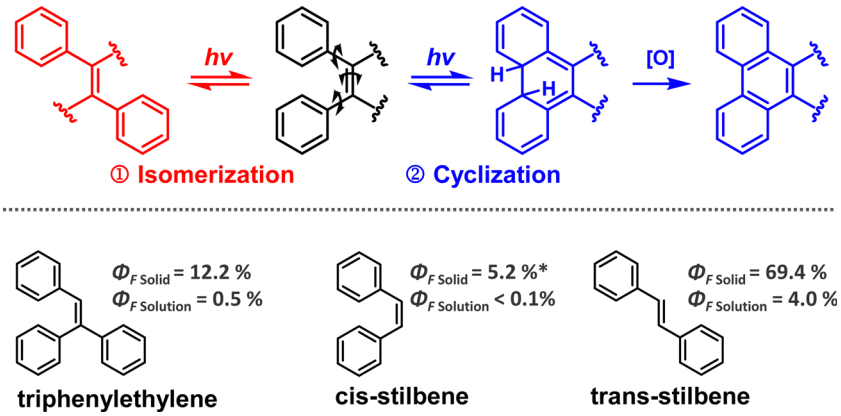

Scheme 1 Photochemical processes of DPE-featured AIE-gens (top panel) and the structures with quantum yields of triphenylethylene, *cis*-stilbene, and *trans*-stilbene (excited with 300 nm, bottom panel). Note that the quantum yield of *cis*-stilbene in the solid state is obtained at 77 K because it is liquid at room temperature.

chosen to explore their AIE mechanism using ultrafast UV/IR spectroscopy and simulations. Among the choices, *trans*-stilbene and *cis*-stilbene are typical molecules for studying photochemical processes experimentally[34–56] and theoretically,[57–73] and triphenylethylene and its derivatives have also attracted attention because of their photochemical properties in recent years.[74–80] The molecular structures and photophysical properties in the solution and those in the solid state are shown in Fig. S1 (ESI†) and Scheme 1. All of them emit much more strongly in solids than in dilute solutions, demonstrating the AIE characteristics. Because the dielectric constant and viscosity of the solvent (DCM or THF) are small, it is reasonable to use gas phase calculations to help study triphenylethylene, *cis*-stilbene, and *trans*-stilbene in the solution.

II. Results and discussion

II.1 Photocyclization of triphenylethylene in solution

The FTIR spectrum of triphenylethylene is displayed in the upper panel of Fig. 1a. From 1250 cm^{-1} to 1650 cm^{-1}, there are three strong vibration absorption peaks, 1446 cm^{-1}, 1493 cm^{-1} and 1599 cm^{-1}, corresponding to the vibrations of the benzene rings. The calculated FTIR spectra of triphenylethylene and its photo-cyclization intermediate 9-phenyl-4*a*,4*b*-dihydrophenanthrene (phenyl-DHP) are displayed in the bottom panel of Fig. 1a. The vibrational frequencies of phenyl-DHP in this range are distinctly different from those of triphenylethylene, which will serve as an indication of cyclization in solutions after photoexcitation in the experiment. Fig. 1b displays the ultrafast transient IR absorption spectra of dilute triphenylethylene solutions after excitation with 300 nm photons at different waiting times. In the solution, after photoexcitation, new absorption peaks appear at 1287 cm^{-1}, 1317 cm^{-1}, 1364 cm^{-1}, 1449 cm^{-1}, 1464 cm^{-1}, 1474 cm^{-1} and 1578 cm^{-1}, which are marked with red arrows in the top panel of Fig. 1b. These peaks closely resemble the calculated peaks of phenyl-DHP, and are distinctly different from those observed in the solid sample in the bottom panel of Fig. 1b. In the solid sample, there are two strong excited-state absorption peaks located at 1437 cm^{-1} and 1484 cm^{-1}, respectively, and a very small peak at 1593 cm^{-1}, which are attributed to the benzene skeleton vibration modes based on their frequency similarity to the corresponding absorption peaks in FTIR (a vibrational absorption peak at an electronically excited state typically has a lower frequency than its counterpart at the electronically ground state). These excited-state absorption peaks belonging to triphenylethylene disappear in the solution. Instead, vibrational absorption peaks attributed to phenyl-DHP appear, indicating the formation of phenyl-DHP in the solution. The spectra in DCM (middle panel of Fig. 1b) are similar to those in THF, consistent with the calculated IR absorption of the cyclic intermediate, phenyl-DHP. All the above results suggest that photocyclization occurs after excitation with 300 nm light in the triphenylethylene solutions.[32,33]

The evolutions of vibrational spectra after photoexcitation in the solid state of triphenylethylene and those in dilute triphenylethylene solutions are compared. As shown in Fig. 2a and b, the partially magnified data in the insets show that in the THF solution, peaks reach maxima at around 3 ps, except for the peak at 1474 cm^{-1} which is affected by the IR absorption of THF.[32] The maxima appear at 1–2 ps in the DCM solution, earlier than that in the THF solution. The results imply that the growth of phenyl-DHP occurs within a few ps. It is known that phenyl-DHP is not stable at room temperature and can reopen the ring and return to the ground state of triphenylethylene, resulting in the decay of signals. A very small portion of phenyl-DHP can be oxidized by oxygen in the solution to form a stable product, which can be detected with GC-MS (Fig. S3, ESI†). The dynamics of the main excited-state absorption peaks in the triphenylethylene solid is different, as shown in Fig. 2c. The peak intensities reach maxima instantaneously after excitation, and then decay rapidly, implying that the signals are not from new structures that require time to grow. The results suggest that no cyclization occurs in the solid state. In addition, the signal of anisotropy peaks remains unchanged within dozens of

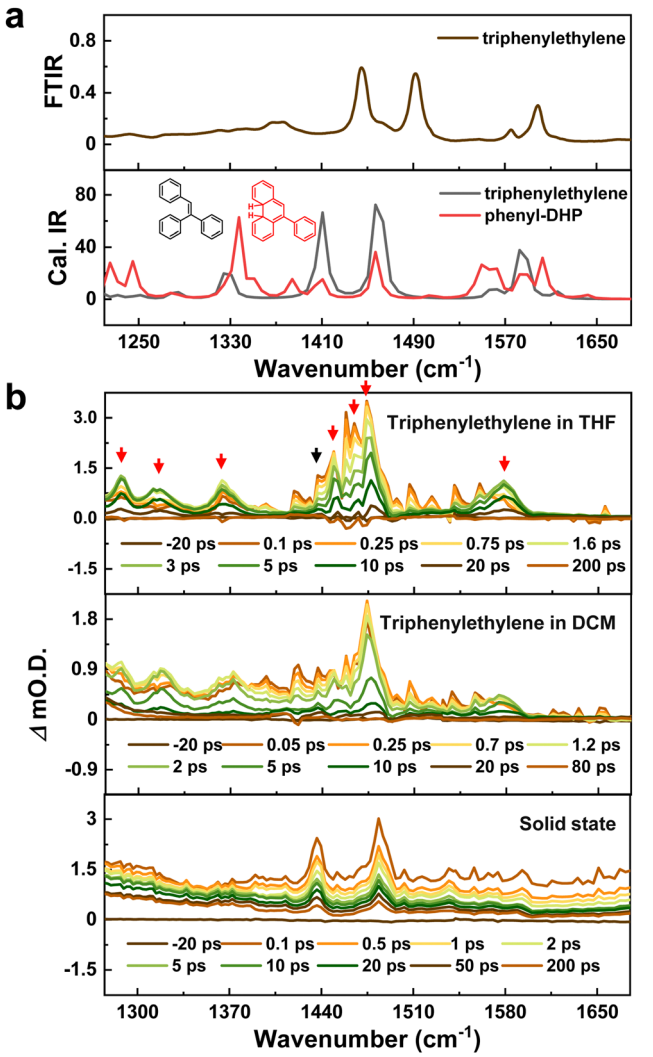

Fig. 1 (a) FTIR spectrum of triphenylethylene and simulated IR spectra of triphenylethylene and phenyl-DHP. (b) Ultrafast UV/IR spectra of triphenylethylene in dilute (100 mM) THF and DCM solutions and in the solid state after excitation with 300 nm.

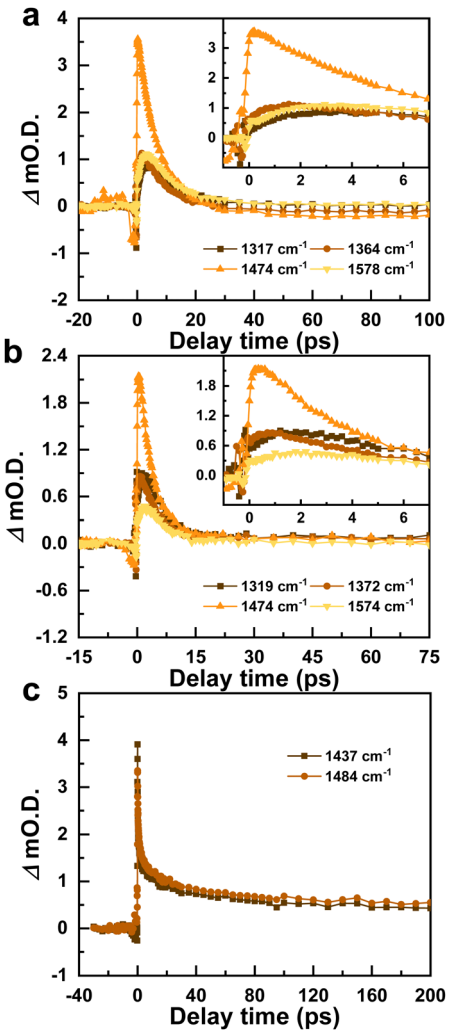

Fig. 2 The evolution of vibrational signals after photo-excitation of triphenylethylene in (a) THF and (b) DCM solutions and (c) in the solid state.

ps (Fig. S2, ESI†), indicating that the energy/charge transfer between molecules is very slow,[32,81] which is probably one of the reasons accounting for the strong fluorescence (no quenching) of triphenylethylene in the solid state.

In Fig. 3 and 4, we present the computational results of ground(S0)/excited(S1) state potential energy curves for photo-excitation of triphenylethylene. The structures along the 1-dimensional path in both Fig. 3a and Fig. 4a are generated by linear interpolation of internal coordinates either from a ground state (S0) minimum to another flipped S0 minimum through a twist-CI point. Because of the chiral conformation, the isomerization of triphenylethylene has two distinctly asymmetric directions, and the barriers are different on the two sides of the twist-CI along the path. As shown in Fig. 3b or Fig. 4b, the structures along the path are produced by linear interpolation of internal coordinates from the triphenylethylene S0 minimum to phenyl-DHP passing a cyclic-CI point. Two multi-reference electronic structure methods are employed for describing electronically ground/excited states. One is the OM2/MRCI method,[82–85] which efficiently combines the semi-empirical OM2 Hamiltonian[82] with multi-reference configuration interaction.[83] The other is the *ab initio* extended multi-state complete active space second-order perturbation theory (XMS-CASPT2),[86] which involves the complete active space self-consistent field (CASSCF)[87] with dynamic electronic correlation by second-order perturbation theory. Both methods are reasonable for describing electronically excited and ground states as well as conical intersections of organic molecules.[84,85,88–90] They are applied in optimizations/calculations of the S0 minimum of triphenylethylene, that of phenyl-DHP, and the cyclic-CI and twist-CI structures in the work. Fig. 3 and 4 demonstrate the S0/S1 potential energy curves produced using OM2/MRCI and XMS-CASPT2, respectively. As shown in Fig. 9, the comparison between CASSCF and XMS-CASPT2 on the S0/S1 potential energy data of the same system indicates that it is important to include dynamic correlation effects for the electronic structure description of the conical intersection regimes.

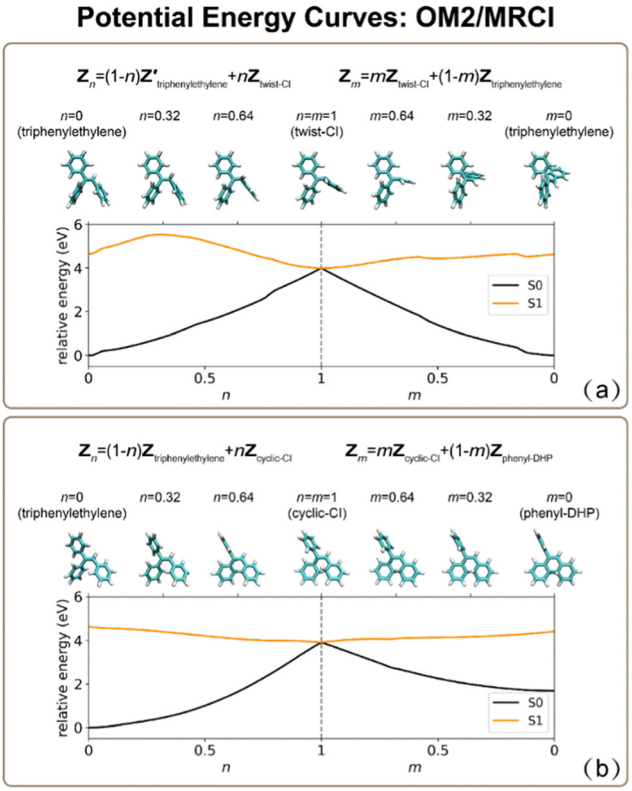

Fig. 3 Potential energy curves of the triphenylethylene system. The molecular structures of triphenylethylene phenyl-DHP and two CIs (twist-CI and cyclic-CI) are optimized using OM2/MRCI. The paths of panel (a) are generated by linear interpolation of internal coordinates from triphenylethylene to twist-CI (left side axis parameterized by $n \in [0,1]$) and from twist-CI to triphenylethylene in another direction (right side axis parameterized by $m \in [0,1]$), while those of panel (b) are generated from triphenylethylene to cyclic-CI (left side axis parameterized by $n \in [0,1]$) and from cyclic-CI to phenyl-DHP (right side axis parameterized by $m \in [0,1]$). The potential energy curves of the ground state (S0) and first excited state (S1) calculated using OM2/MRCI are demonstrated as black and orange solid lines, respectively, where the zero value is set to the S0 minimum of triphenylethylene. Note that, in panel (a), $Z_{triphenylethylene}$ (for n = 0) and $Z'_{triphenylethylene}$ (for m = 0) share the same chemical structure but have different internal coordinates because the labeling order of the atoms is different before and after the isomerization. Several molecular geometries along the paths are selected for demonstration.

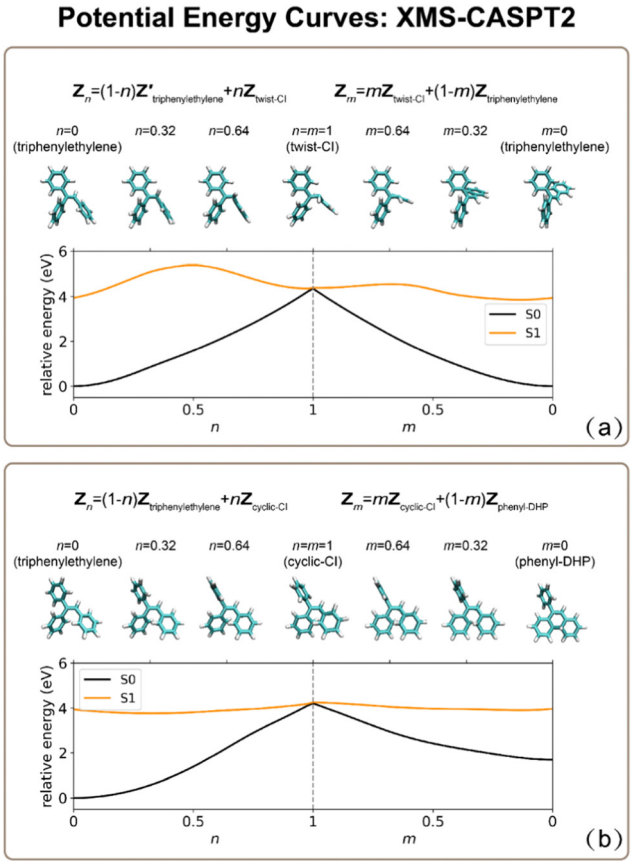

Fig. 4 Same as Fig. 3, but produced using the XMS-CASPT2(2,2)/cc-pVDZ method.

Upon being vertically excited, triphenylethylene has two relaxation pathways through two CIs, the cyclic-CI and the twist-CI, where the electronically excited and ground states have the same potential energy. In the CI region, the electronically excited energy can be rapidly converted to vibrational/rotational energy in the form of non-radiative transitions back to the ground electronic state of triphenylethylene or that of the photocyclized or isomerized product. The electronically excited state dynamics of the entire process depends on the barrier encountered before approaching the CI region. As shown in Fig. 3a or Fig. 4a, the barrier before approaching the cyclic-CI region is expected to be relatively small, which implies that crossing the cyclic-CI is fast,[91,92] within several ps as observed experimentally, two to three orders of magnitude faster than the typical radiative transition time scale of ~ns. Therefore, most of the excited energy has been dissipated in the form of non-radiative transitions *via* crossing CI before emission occurs, leading to a very low quantum yield in the triphenylethylene solution (less than 1%). It is likely for triphenylethylene to cross both CIs, but since there is no change in the molecular structure at the ground electronic state before and after isomerization (twist-CI), the experimental results presented here can only verify the process of crossing the cyclic-CI. In the solid state, the triphenylethylene system also has both CIs. However, the structural evolution from the vertically excited structure to either CI requires twisting and rotation of the benzene rings. The close and rigid molecular packing in the solid imposes extra energy costs for these motions to proceed, compared to those in the liquids where nearby molecules are mobile. Therefore, it is much slower for the excited triphenylethylene system to reach CIs in the solid state, which can be even slower than the spontaneous emission (fluorescence), and thereby the emission quantum yield is not significantly affected.

II.2 Isomerization of stilbene in solution

cis-Stilbene and *trans*-stilbene are two other DPE-featured AIEgens. Their FTIR (top panel) and calculated IR spectra (bottom panel) in the range of 1300–1700 cm^{-1} are displayed in Fig. 5a,

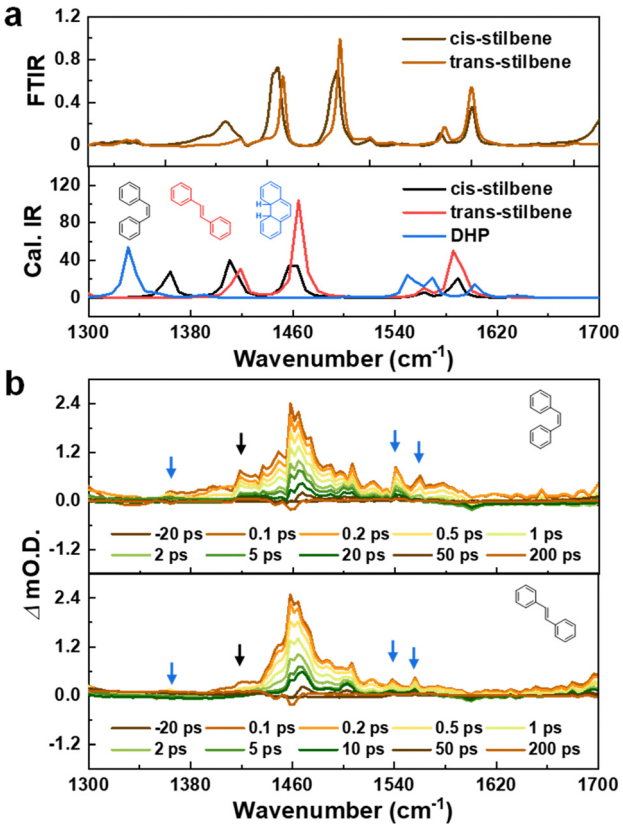

Fig. 5 (a) FTIR spectra of *cis*-stilbene and *trans*-stilbene, and calculated IR spectra of *cis*-stilbene, *trans*-stilbene and DHP. (b) Ultrafast UV/IR spectra after excitation with 300 nm light of *cis*-stilbene and *trans*-stilbene in dilute THF solutions (100 mM).

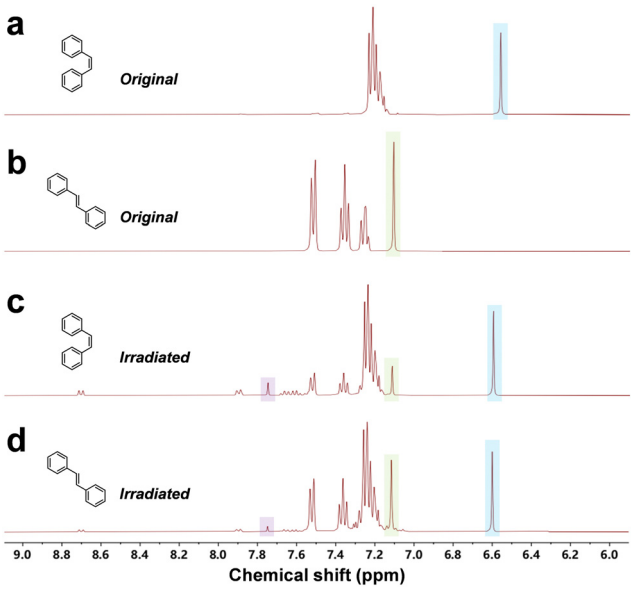

Fig. 6 ^{1}H NMR spectra of *cis*-stilbene and *trans*-stilbene (a and b) before and (c and d) after irradiation with 300 nm light in $CDCl_3$ for 12 h.

along with the calculated IR spectrum (bottom panel) of the cyclic intermediate of *cis*-stilbene, 4*a*,4*b*-dihydrophenanthrene (DHP). As for *cis*-stilbene and *trans*-stilbene, both calculated and experimental infrared spectra are similar. Because DHP is not stable, the experimental infrared spectrum is not available in this work. The simulation results suggest that DHP does not have absorption peaks between 1400 cm^{-1} and 1500 cm^{-1} as stilbene has. Instead, the peaks of DHP appear below 1400 cm^{-1} and above 1500 cm^{-1}.

The ultrafast UV/IR spectra at different delay times were collected with 300 nm excitation of *cis*-stilbene or *trans*-stilbene in THF (100 mM) (Fig. 5b). Both systems have two excited-state absorption peaks at around 1464 cm^{-1} and 1503 cm^{-1}, and a small bleaching peak at 1600 cm^{-1}, corresponding to the three main peaks in FTIR. The intensities of peaks at 1360 cm^{-1}, 1420 cm^{-1}, and 1540–1550 cm^{-1} (marked with blue and black arrows) are significantly stronger in *cis*-stilbene than in *trans*-stilbene. According to the FTIR spectra and computational results mentioned above, a small amount of cyclic intermediate DHP (1360 cm^{-1} and 1550 cm^{-1}) is generated after irradiation. The absorption peaks (around 1420 cm^{-1}) after photo-excitation in the *trans*-stilbene solution can be assigned to *cis*-stilbene, which undoubtedly indicates the photo-isomerization from *trans*-stilbene to *cis*-stilbene. In principle, *cis*-stilbene can also isomerize to *trans*-stilbene, but it is not easy to identify *via* UV/IR spectroscopy due to peak overlapping.

Furthermore, ^{1}H NMR spectra are used to analyze the isomerization of stilbene. The ^{1}H NMR spectra of *cis*-stilbene and *trans*-stilbene solutions in $CDCl_3$ are collected before and after irradiation with 300 nm light (Fig. 6). The resonance peaks at 6.6 ppm and 7.1 ppm (shaded in light green and blue) associated with the two H atoms connected to the central C=C of *cis*-stilbene and *trans*-stilbene, respectively, are used to represent the compositional change after irradiation. The peak at 7.75 ppm (shaded in light purple) belongs to the oxidation product (phenanthrene) of the cyclic intermediate product, DHP. The percentage of each component is calculated from the proportional relationship of these singlet peak areas. Specifically, after 12 h of irradiation with 300 nm light, *trans*-stilbene and phenanthrene are produced in the *cis*-stilbene solution, and the ratio of *cis*-stilbene/*trans*-stilbene/phenanthrene is 60/27/13. The ratio in the *trans*-stilbene solution is 48/48/4. The above results are also verified by GC-MS (Fig. S4, ESI†). The results imply that it is relatively easier for *trans*-stilbene to convert into *cis*-stilbene during isomerization.

Similarly, we optimized the ground-state (S0) minimum of *trans*/*cis*-stilbene, DHP, and two CI structures (the twist-CI in isomerization and the cyclic-CI in cyclization). The S0/S1 energy curves and selected molecular geometries along the linearly interpolated paths are shown in Fig. 7 and 8, produced using OM2/MRCI and XMS-CASPT2, respectively. This shows that after excitation the *trans*-stilbene system can reach the twist-CI, and then either return to its ground state or isomerize to *cis*-stilbene. In comparison, after photo-excitation, the *cis*-stilbene system has not only the isomerization path (through the twist-CI region) to yield *trans*-stilbene, but also the cyclization path (the cyclic-CI region) to produce DHP. After cyclization, the

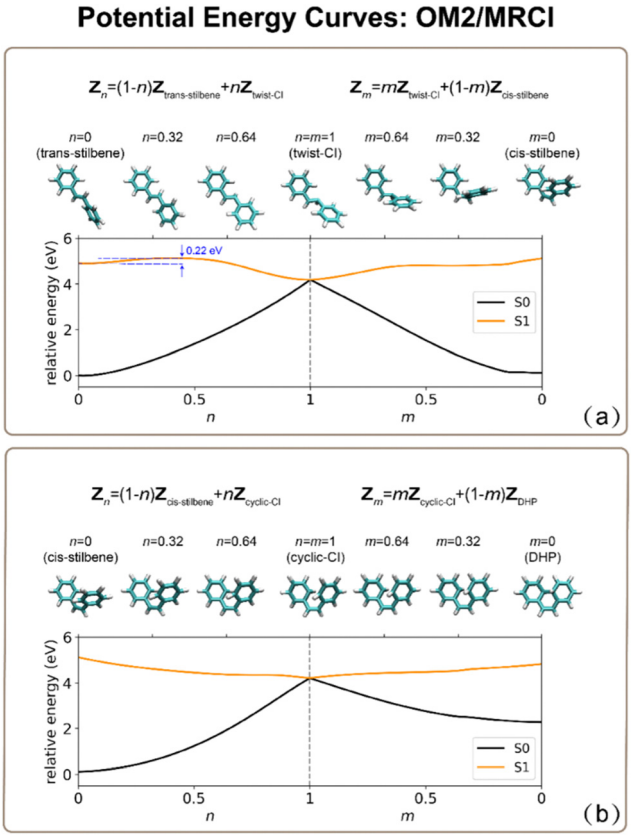

Fig. 7 Potential energy curves of stilbene. The molecular structure of *cis*-stilbene, *trans*-stilbene, DHP, and two conical intersection structures (twist-CI and cyclic-CI) are optimized using the OM2/MRCI method. The paths in panel (a) are generated by linear interpolation of internal coordinates from *trans*-stilbene to twist-CI (left side axis parameterized by $n \in [0,1]$) and from twist-CI to *cis*-stilbene (right side axis parameterized by $m \in [0,1]$), while those in panel (b) are generated from *cis*-stilbene to cyclic-CI (left side axis parameterized by $n \in [0,1]$) and from cyclic-CI to DHP (right side axis parameterized by $n \in [0,1]$). The potential energy curves of the ground state (S0) and first excited state (S1) calculated using OM2/MRCI are demonstrated as black and orange solid lines in each panel, respectively, where the zero value is set to the S0 minimum of *trans*-stilbene. Several molecular geometries along the paths are selected for demonstration.

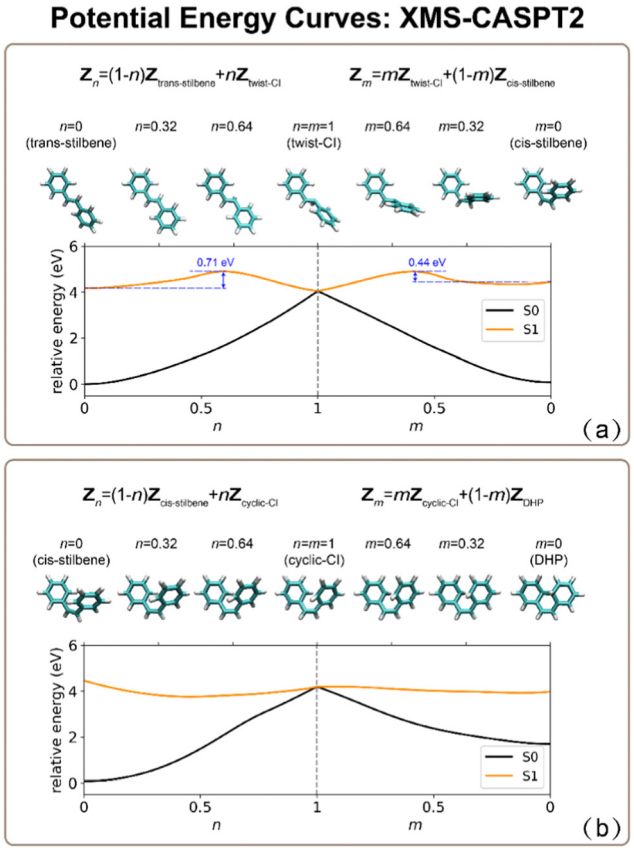

Fig. 8 Same as Fig. 7, but produced by the XMS-CASPT2(2,2)/cc-pVDZ method.

resulting intermediate DHP may gradually reopen the ring structure to form *cis*-stilbene,[93] and such a process is confirmed in previous nonadiabatic dynamics simulations, which show a considerable ratio of the intermediate DHP returning to *cis*-stilbene.[72] In addition, the computational results (by either OM2/MRCI or XMS-CASPT2) suggest that the energy barriers for reaching both CIs in the *cis*-stilbene system are lower than that for approaching the twist-CI in the *trans*-stilbene, implying that it is much easier and faster for *cis*-stilbene to cross the CI regions than *trans*-stilbene, resulting in a much lower fluorescence quantum yield of *cis*-stilbene as experimentally observed. The quantitative ratios of interconversion processes after long-time irradiation may be explored with nonadiabatic dynamics on a long-time scale, for which computational methods (such as phase space mapping approaches[94–96]) could be considered in future studies.

III. Concluding remarks

In summary, both experimental and computational results suggest that three DPE-featured AIE-gens, triphenylethylene, *cis*-stilbene, and *trans*-stilbene can rapidly reach CIs and non-radiatively dissipate electronic energy in dilute solutions on the time scale of ps, resulting in very low fluorescence quantum yields. In the solid state, however, the structural evolution is limited by the closely packed surrounding molecules. The molecule can hardly approach CIs after photoexcitation. Without such a fast energy dissipation pathway by crossing CIs, and with the aid of the non-planar structure and the long intermolecular distances which prevent electron or energy transfers between adjacent molecules, AIE molecules in solids can avoid quenching and emit strongly. The mechanism of crossing CIs also well explains the differences in fluorescence quantum yields of *cis*-stilbene and *trans*-stilbene.

IV. Experimental methods

Sample preparation

Triphenylethylene (>98%), *cis*-stilbene (>96%), and *trans*-stilbene (>98%) were purchased from Aladdin, Bidepharm (Shanghai, China), and Konoscience (Beijing, China), respectively. All the solvents were of HPLC grade purchased from Concord Technology (Tianjin, China).

Optical experiments

The UV-vis spectra were collected with a UV-3600Plus UV-vIS-NIR spectrometer (Shimadzu Inc). The fluorescence spectra and absolute quantum yields were measured with an FLS980 spectrometer with an integrating sphere (Edingburgh Instruments Inc).

The ultraviolet/infrared (UV/IR) mixed frequency ultrafast spectra were collected using a method similar to that in our reported work.[32] The UV excitation power 300 nm was ~100 μW with a spot diameter of 245.3 μm and a sample cell thickness of 50 μm for solutions.

GC-MS characterization

Gas chromatography-mass (GC-MS) analyses were carried out on a gas chromatography system coupled to an electrostatic orbitrap mass spectrometer (ThermoFisher, Q Exactive GC) equipped with an electrospray ionization (EI) source by using a TG-5HT column (30 m, 0.25 mm, 0.25 μm). The analytes were eluted with He gas at a flow rate of 1.0 mL min^{-1}.

Theoretical calculation

In the simulation of the vibrational spectrum of the ground electronic state, the geometry optimizations and corresponding vibrational frequencies estimations were carried out with the M06-2X density functional[97] and def2-TZVP basis set.[98] All the

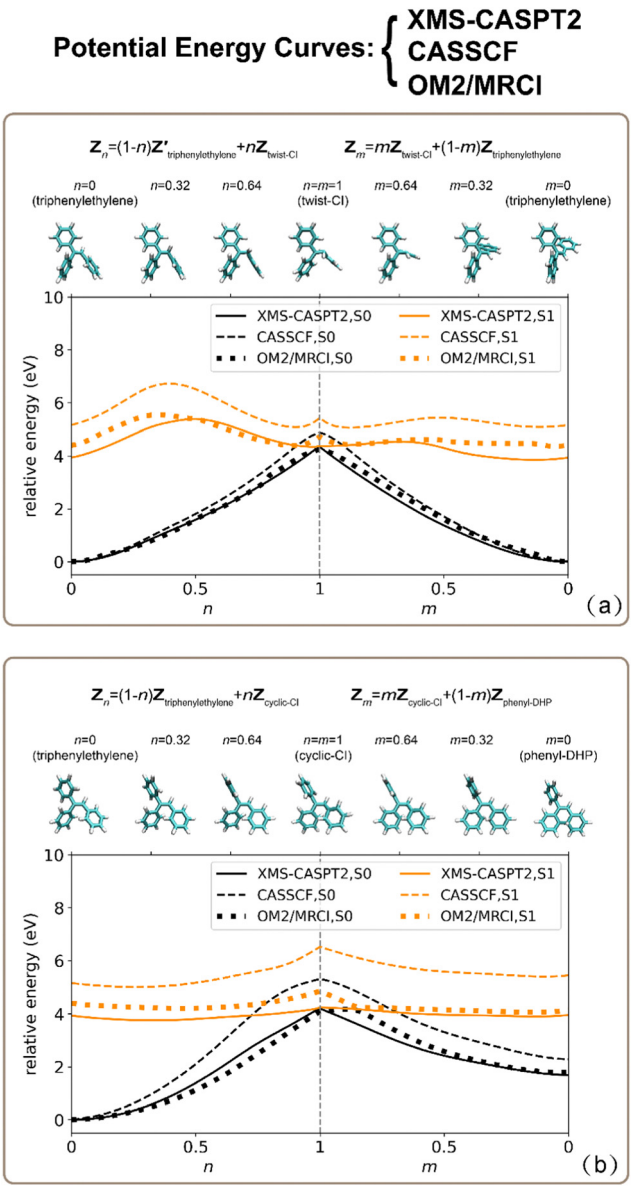

Fig. 9 Same as Fig. 4. The molecular structures produced using XMS-CASPT2(2,2)/cc-pVDZ are used to show the differences among the three electronic structure methods. The CASSCF(2,2)/cc-pVDZ potential energy curves of the ground and excited state are shown as black and orange dashed lines, respectively. In addition, the OM2/MRCI potential energy curves of the ground and excited state are demonstrated as black and orange dotted lines, respectively.

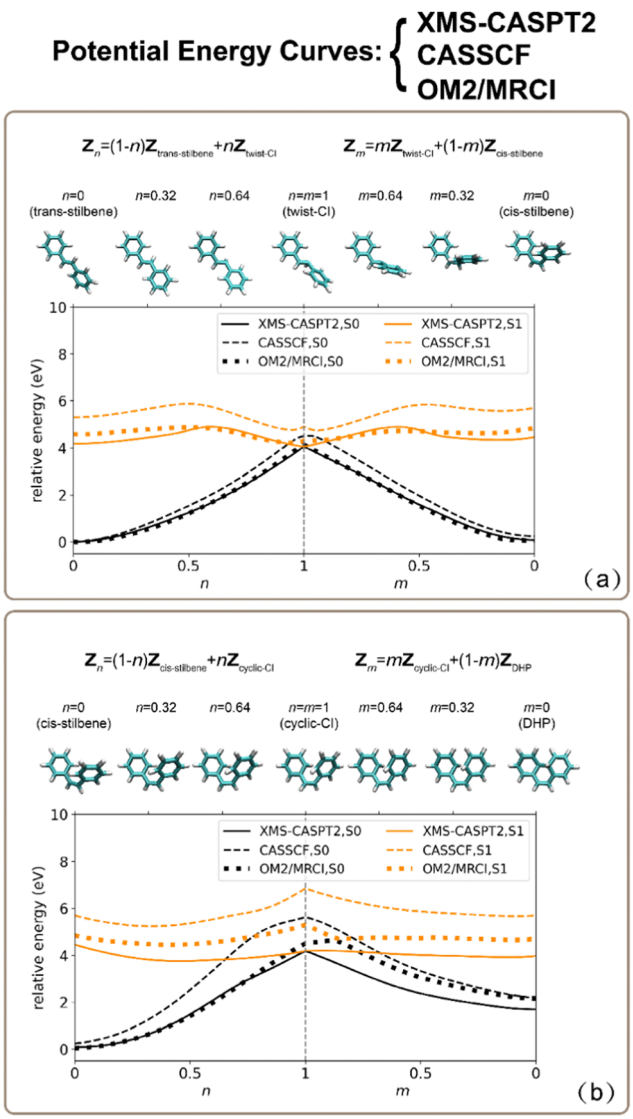

Fig. 10 Same as Fig. 8. The molecular structures produced by XMS-CASPT2(2,2)/cc-pVDZ are used to show the differences among the three electronic structure methods. The CASSCF(2,2)/cc-pVDZ potential energy curves of the ground and excited state are demonstrated as black and orange dashed lines, respectively. The OM2/MRCI potential energy curves of the ground and excited state are depicted as black and orange dotted lines, respectively.

DFT calculations for triphenylethylene and phenyl-DHP in Fig. 1(a), and for *cis*-stilbene, *trans*-stilbene, and DHP in Fig. 5(a) were performed with the Gaussian 16 software.[99] A scaling factor of 0.946 was used to produce these vibrational spectra.[100–102]

All OM2/MRCI[82–84] calculations were carried out with the MNDO program.[103] The restricted open-shell Hartree-Fock (ROHF) formalism was used in the self-consistent field treatment. Molecular orbitals were obtained using the OM2 semiempirical Hamiltonian. The active space included 6 occupied orbitals and 4 virtual orbitals. During OM2/MRCI geometry optimizations, all required energies, gradients, and nonadiabatic coupling elements were computed by the multireference configuration interaction using the graphical unitary group approach (GUGA).[83] The path between optimized structures was obtained by the linear interpolation of internal coordinates.

The XMS-CASPT2 calculations were carried out with the BAGEL program.[104,105] The active space was chosen as (2,2) for describing the $\pi \rightarrow \pi^*$ excitation.[72] The electronic basis set was chosen as cc-pVDZ[106] and the corresponding density fitting basis set is available in BAGEL. The paths used for demonstration in Fig. 4 and 8 were obtained by linear interpolation of internal coordinates of optimized structures from XMS-CASPT2 calculations. The corresponding CASSCF potential energy curves and OM2/MRCI potential energy curves of the same path of Fig. 4 (or Fig. 8) are also demonstrated in Fig. 9 (or Fig. 10). In comparison, the CASSCF excited state potential energy curves differ significantly from those of XMS-CASPT2, particularly around the CIs, which indicates that dynamic electronic correlation effects are essential for describing the excited states of stilbene and triphenylethylene around CIs. The OM2/MRCI method is more appropriate for describing CIs of stilbene and triphenylethylene than CASSCF, yielding similar results to the XMS-CASPT2 data.

Conflicts of interest

There are no conflicts to declare.

Acknowledgements

We acknowledge financial support from the National Science Foundation of China (NSFC-21627805, 22225304, 21927901, 21925501, 12174012, 21821004, and 21961142017) and the Ministry of Science and Technology of China (MOST) grant no. 2017YFA0204901. We thank the High-performance Computing Platform of Peking University, Beijing PARATERA Tech Co., Ltd, and the Guangzhou supercomputer center for providing computational resources. This work was partially supported by the Analytical Instrument Center of Peking University.

References

1 X. Yang, G. Zhou and W.-Y. Wong, *Chem. Soc. Rev.*, 2015, **44**, 8484–8575, DOI: **10.1039/C5CS00424A**.
2 Y. Zhang, Y. Wang, J. Song, J. Qu, B. Li, W. Zhu and W.-Y. Wong, *Adv. Opt. Mater.*, 2018, **6**, 1800466, DOI: **10.1002/adom.201800466**.
3 J. Yang and Q. Peng, *Chin. J. Chem. Phys.*, 2022, **35**, 38–51, DOI: **10.1063/1674-0068/cjcp2112281**.
4 Y.-L. Ji and Q.-S. Li, *Chin. J. Chem. Phys.*, 2022, **35**, 499–508, DOI: **10.1063/1674-0068/cjcp2203039**.
5 J. R. Lakowicz, *Principles of Fluorescence Spectroscopy*, Springer, New York, 2006.
6 J. Luo, Z. Xie, J. W. Y. Lam, L. Cheng, H. Chen, C. Qiu, H. S. Kwok, X. Zhan, Y. Liu, D. Zhu and B. Z. Tang, *Chem. Commun.*, 2001, 1740–1741, DOI: **10.1039/B105159H**.
7 Y. Hong, J. W. Y. Lam and B. Z. Tang, *Chem. Commun.*, 2009, 4332–4353, DOI: **10.1039/B904665H**.
8 Y. Hong, J. W. Y. Lam and B. Z. Tang, *Chem. Soc. Rev.*, 2011, **40**, 5361–5388, DOI: **10.1039/C1CS15113D**.
9 J. Mei, Y. Hong, J. W. Y. Lam, A. Qin, Y. Tang and B. Z. Tang, *Adv. Mater.*, 2014, **26**, 5429–5479, DOI: **10.1002/adma.201401356**.
10 J. Mei, N. L. C. Leung, R. T. K. Kwok, J. W. Y. Lam and B. Z. Tang, *Chem. Rev.*, 2015, **115**, 11718–11940, DOI: **10.1021/acs.chemrev.5b00263**.
11 E. E. Jelley, *Nature*, 1936, **138**, 1009–1010, DOI: **10.1038/1381009a0**.
12 J. I. Zink, G. E. Hardy and J. E. Sutton, *J. Phys. Chem.*, 1976, **80**, 248–249, DOI: **10.1021/j100544a007**.
13 G. Fischer, E. Fischer and H. Stegemeyer, *Ber. Bunsenges. Phys. Chem.*, 1973, **77**, 685–687, DOI: **10.1002/bbpc.19730770907**, **https://onlinelibrary.wiley.com/doi/abs/10.1002/bbpc.19730770907**.
14 F. Bu, E. Wang, Q. Peng, R. Hu, A. Qin, Z. Zhao and B. Z. Tang, *Chem. – Eur. J.*, 2015, **21**, 4440–4449, DOI: **10.1002/chem.201405902**.
15 J. Sturala, M. K. Etherington, A. N. Bismillah, H. F. Higginbotham, W. Trewby, J. A. Aguilar, E. H. C. Bromley, A.-J. Avestro, A. P. Monkman and P. R. McGonigal, *J. Am. Chem. Soc.*, 2017, **139**, 17882–17889, DOI: **10.1021/jacs.7b08570**.
16 S. Chen, W. Li, X. Li and W.-H. Zhu, *J. Mater. Chem. C*, 2017, **5**, 2717–2722, DOI: **10.1039/C7TC00023E**.
17 N. Sinha, L. Stegemann, T. T. Y. Tan, N. L. Doltsinis, C. A. Strassert and F. E. Hahn, *Angew. Chem., Int. Ed.*, 2017, **56**, 2785–2789, DOI: **10.1002/anie.201610971**.
18 N. L. C. Leung, N. Xie, W. Yuan, Y. Liu, Q. Wu, Q. Peng, Q. Miao, J. W. Y. Lam and B. Z. Tang, *Chem. – Eur. J.*, 2014, **20**, 15349–15353, DOI: **10.1002/chem.201403811**.
19 J. Chen, C. C. W. Law, J. W. Y. Lam, Y. Dong, S. M. F. Lo, I. D. Williams, D. Zhu and B. Z. Tang, *Chem. Mater.*, 2003, **15**, 1535–1546, DOI: **10.1021/cm021715z**.
20 D. A. Shultz and M. A. Fox, *J. Am. Chem. Soc.*, 1989, **111**, 6311–6320, DOI: **10.1021/ja00198a049**.
21 X.-L. Peng, S. Ruiz-Barragan, Z.-S. Li, Q.-S. Li and L. Blancafort, *J. Mater. Chem. C*, 2016, **4**, 2802–2810, DOI: **10.1039/C5TC03322E**.
22 Q. Li and L. Blancafort, *Chem. Commun.*, 2013, **49**, 5966–5968, DOI: **10.1039/C3CC41730A**.

23 Y.-J. Gao, X.-P. Chang, X.-Y. Liu, Q.-S. Li, G. Cui and W. Thiel, *J. Phys. Chem. A*, 2017, **121**, 2572–2579, DOI: 10.1021/acs.jpca.7b00197.
24 J. A. Snyder and A. E. Bragg, *J. Phys. Chem. Lett.*, 2018, **9**, 5847–5854, DOI: 10.1021/acs.jpclett.8b02489.
25 Z. Zhou, S. Xie, X. Chen, Y. Tu, J. Xiang, J. Wang, Z. He, Z. Zeng and B. Z. Tang, *J. Am. Chem. Soc.*, 2019, **141**, 9803–9807, DOI: 10.1021/jacs.9b04426.
26 J.-B. Xiong, Y.-X. Yuan, L. Wang, J.-P. Sun, W.-G. Qiao, H.-C. Zhang, M. Duan, H. Han, S. Zhang and Y.-S. Zheng, *Org. Lett.*, 2018, **20**, 373–376, DOI: 10.1021/acs.orglett.7b03662.
27 K. Kokado, T. Machida, T. Iwasa, T. Taketsugu and K. Sada, *J. Phys. Chem. C*, 2018, **122**, 245–251, DOI: 10.1021/acs.jpcc.7b11248.
28 Y. Cai, L. Du, K. Samedov, X. Gu, F. Qi, H. H. Y. Sung, B. O. Patrick, Z. Yan, X. Jiang, H. Zhang, J. W. Y. Lam, I. D. Williams, D. Lee Phillips, A. Qin and B. Z. Tang, *Chem. Sci.*, 2018, **9**, 4662–4670, DOI: 10.1039/C8SC01170B.
29 L. Le Bras, C. Adamo and A. Perrier, *J. Phys. Chem. C*, 2017, **121**, 25603–25616, DOI: 10.1021/acs.jpcc.7b09310.
30 Q. Peng and Z. Shuai, *Aggregate*, 2021, **2**, e91, DOI: 10.1002/agt2.91.
31 R. Crespo-Otero, Q. Li and L. Blancafort, *Chem. – Asian J.*, 2019, **14**, 700–714, DOI: 10.1002/asia.201801649.
32 J. Guan, R. Wei, A. Prlj, J. Peng, K.-H. Lin, J. Liu, H. Han, C. Corminboeuf, D. Zhao, Z. Yu and J. Zheng, *Angew. Chem., Int. Ed.*, 2020, **59**, 14903–14909, DOI: 10.1002/anie.202004318.
33 J. Guan, C. Shen, J. Peng and J. Zheng, *J. Phys. Chem. Lett.*, 2021, **12**, 4218–4226, DOI: 10.1021/acs.jpclett.0c03861.
34 G. N. Lewis, T. T. Magel and D. Lipkin, *J. Am. Chem. Soc.*, 1940, **62**, 2973–2980, DOI: 10.1021/ja01868a024.
35 W. M. Moore, D. D. Morgan and F. R. Stermitz, *J. Am. Chem. Soc.*, 1963, **85**, 829–830, DOI: 10.1021/ja00889a050.
36 K. A. Muszkat and E. Fischer, *J. Chem. Soc. B*, 1967, 662–678, DOI: 10.1039/j29670000662.
37 J. Saltiel, *J. Am. Chem. Soc.*, 1967, **89**, 1036–1037, DOI: 10.1021/ja00980a057.
38 B. I. Greene, R. M. Hochstrasser and R. B. Weisman, *Chem. Phys.*, 1980, **48**, 289–298, DOI: 10.1016/0301-0104(80)80059-0.
39 A. B. Myers and R. A. Mathies, *J. Chem. Phys.*, 1984, **81**, 1552–1558, DOI: 10.1063/1.447884.
40 F. E. Doany, R. M. Hochstrasser, B. I. Greene and R. R. Millard, *Chem. Phys. Lett.*, 1985, **118**, 1–5, DOI: 10.1016/0009-2614(85)85254-4.
41 S. Abrash, S. Repinec and R. M. Hochstrasser, *J. Chem. Phys.*, 1990, **93**, 1041–1053, DOI: 10.1063/1.459168.
42 H. Petek, K. Yoshihara, Y. Fujiwara, L. Zhe, J. H. Penn and J. H. Frederick, *J. Phys. Chem.*, 1990, **94**, 7539–7543, DOI: 10.1021/j100382a043.
43 D. H. Waldeck, *Chem. Rev.*, 1991, **91**, 415–436, DOI: 10.1021/cr00003a007.
44 J. Saltiel, A. S. Waller and D. F. Sears, *J. Am. Chem. Soc.*, 1993, **115**, 2453–2465, DOI: 10.1021/ja00059a047.
45 R. J. Sension, S. T. Repinec, A. Z. Szarka and R. M. Hochstrasser, *J. Chem. Phys.*, 1993, **98**, 6291–6315, DOI: 10.1063/1.464824.
46 D. C. Todd and G. R. Fleming, *J. Chem. Phys.*, 1993, **98**, 269–279, DOI: 10.1063/1.464672.
47 C. Warmuth, F. Milota, H. F. Kauffmann, H. Wadi and E. Pollak, *J. Chem. Phys.*, 2000, **112**, 3938–3941, DOI: 10.1063/1.480993.
48 W. Fuss, C. Kosmidis, W. E. Schmid and S. A. Trushin, *Angew. Chem., Int. Ed.*, 2004, **43**, 4178–4182, DOI: 10.1002/anie.200454221.
49 K. Ishii, S. Takeuchi and T. Tahara, *Chem. Phys. Lett.*, 2004, **398**, 400–406, DOI: 10.1016/j.cplett.2004.09.075.
50 S. Takeuchi, S. Ruhman, T. Tsuneda, M. Chiba, T. Taketsugu and T. Tahara, *Science*, 2008, **322**, 1073–1077, DOI: 10.1126/science.1160902.
51 M. Sajadi, A. L. Dobryakov, E. Garbin, N. P. Ernsting and S. A. Kovalenko, *Chem. Phys. Lett.*, 2010, **489**, 44–47, DOI: 10.1016/j.cplett.2010.02.034.
52 T. Nakamura, S. Takeuchi, T. Taketsugu and T. Tahara, *Phys. Chem. Chem. Phys.*, 2012, **14**, 6225–6232, DOI: 10.1039/c2cp23959k.
53 S. A. Kovalenko, A. L. Dobryakov, E. Pollak and N. P. Ernsting, *J. Chem. Phys.*, 2013, **139**, 011101, DOI: 10.1063/1.4812776.
54 M. Quick, A. L. Dobryakov, I. N. Ioffe, A. A. Granovsky, S. A. Kovalenko and N. P. Ernsting, *J. Phys. Chem. Lett.*, 2016, **7**, 4047–4052, DOI: 10.1021/acs.jpclett.6b01923.
55 J. Syage, W. R. Lambert, P. Felker, A. Zewail and R. Hochstrasser, *Chem. Phys. Lett.*, 1982, **88**, 266–270, DOI: 10.1016/0009-2614(82)87085-1.
56 T. Baumert, T. Frohnmeyer, B. Kiefer, P. Niklaus, M. Strehle, G. Gerber and A. Zewail, *Appl. Phys. B*, 2001, **72**, 105–108, DOI: 10.1007/s003400000497.
57 G. Orlandi and W. Siebrand, *Chem. Phys. Lett.*, 1975, **30**, 352–354, DOI: 10.1016/0009-2614(75)80005-4.
58 E. Pollak, *J. Chem. Phys.*, 1987, **86**, 3944–3949, DOI: 10.1063/1.451903.
59 J. Troe and K. M. Weitzel, *J. Chem. Phys.*, 1988, **88**, 7030–7039, DOI: 10.1063/1.454402.
60 G. Gershinsky and E. Pollak, *J. Chem. Phys.*, 1996, **105**, 4388–4390, DOI: 10.1063/1.472256.
61 M. J. Bearpark, F. Bernardi, S. Clifford, M. Olivucci, M. A. Robb and T. Vreven, *J. Phys. Chem. A*, 1997, **101**, 3841–3847, DOI: 10.1021/jp961509c.
62 G. Gershinsky and E. Pollak, *J. Chem. Phys.*, 1997, **107**, 10532–10538, DOI: 10.1063/1.474217.
63 G. Gershinsky and E. Pollak, *J. Chem. Phys.*, 1997, **107**, 812–824, DOI: 10.1063/1.474381.
64 C. D. Berweger, W. F. van Gunsteren and F. Muller-Plathe, *J. Chem. Phys.*, 1998, **108**, 8773–8781, DOI: 10.1063/1.475397.
65 G. Gershinsky and E. Pollak, *J. Chem. Phys.*, 1998, **108**, 9186–9187, DOI: 10.1063/1.476365.
66 Y. Amatatsu, *Chem. Phys. Lett.*, 1999, **314**, 364–368, DOI: 10.1016/S0009-2614(99)01042-8.
67 Y. S. Dou and R. E. Allen, *J. Chem. Phys.*, 2003, **119**, 10658–10666, DOI: 10.1063/1.1621621.
68 Y. S. Dou and R. E. Allen, *J. Mod. Optic.*, 2004, **51**, 2485–2491, DOI: 10.1080/09500340408231807.

69 J. Tatchen and E. Pollak, *J. Chem. Phys.*, 2008, **128**, 164303, DOI: 10.1063/1.2895041.
70 Y. Harabuchi, R. Yamamoto, S. Maeda, S. Takeuchi, T. Tahara and T. Taketsugu, *J. Phys. Chem. A*, 2016, **120**, 8804–8812, DOI: 10.1021/acs.jpca.6b07548.
71 Y. Liu, S. H. Xia and Y. Zhang, *Chem. Phys.*, 2020, **539**, 110957, DOI: 10.1016/j.chemphys.2020.110957.
72 H. Weir, M. Williams, R. M. Parrish, E. G. Hohenstein and T. J. Martinez, *J. Phys. Chem. B*, 2020, **124**, 5476–5487, DOI: 10.1021/acs.jpcb.0c03344.
73 M. Williams, R. Forbes, H. Weir, K. Veyrinas, R. J. MacDonell, A. E. Boguslavskiy, M. S. Schuurman, A. Stolow and T. J. Martinez, *J. Phys. Chem. Lett.*, 2021, **12**, 6363–6369, DOI: 10.1021/acs.jpclett.1c01227.
74 Z. Yang, Z. Chi, T. Yu, X. Zhang, M. Chen, B. Xu, S. Liu, Y. Zhang and J. Xu, *J. Mater. Chem.*, 2009, **19**, 5541–5546, DOI: 10.1039/B902802A.
75 W. Qin, Z. Yang, Y. Jiang, J. W. Y. Lam, G. Liang, H. S. Kwok and B. Z. Tang, *Chem. Mater.*, 2015, **27**, 3892–3901, DOI: 10.1021/acs.chemmater.5b00568.
76 D. Ou, T. Yu, Z. Yang, T. Luan, Z. Mao, Y. Zhang, S. Liu, J. Xu, Z. Chi and M. R. Bryce, *Chem. Sci.*, 2016, **7**, 5302–5306, DOI: 10.1039/c6sc01205a.
77 C. Wang, L. Li, X. Zhan, Z. Ruan, Y. Xie, Q. Hu, S. Ye, Q. Li and Z. Li, *Sci. Bull.*, 2016, **61**, 1746–1755, DOI: 10.1007/s11434-016-1180-1.
78 B. Xu, Y. Mu, Z. Mao, Z. Xie, H. Wu, Y. Zhang, C. Jin, Z. Chi, S. Liu, J. Xu, Y.-C. Wu, P.-Y. Lu, A. Lien and M. R. Bryce, *Chem. Sci.*, 2016, **7**, 2201–2206, DOI: 10.1039/C5SC04155D.
79 Z. Zhao, S. Gao, X. Zheng, P. Zhang, W. Wu, R. T. K. Kwok, Y. Xiong, N. L. C. Leung, Y. Chen, X. Gao, J. W. Y. Lam and B. Z. Tang, *Adv. Funct. Mater.*, 2018, **28**, 1705609, DOI: 10.1002/adfm.201705609.
80 N. Li, Y. Gu, Y. Chen, L. Zhang, Q. Zeng, T. Geng, L. Wu, L. Jiang, G. Xiao, K. Wang and B. Zou, *J. Phys. Chem. C*, 2019, **123**, 6763–6767, DOI: 10.1021/acs.jpcc.9b00670.
81 A. F. Fidler, V. P. Singh, P. D. Long, P. D. Dahlberg and G. S. Engel, *J. Chem. Phys.*, 2013, **139**, 155101, DOI: 10.1063/1.4824637.
82 W. Weber and W. Thiel, *Theor. Chem. Acc.*, 2000, **103**, 495–506, DOI: 10.1007/s002149900083.
83 A. Koslowski, M. E. Beck and W. Thiel, *J. Comput. Chem.*, 2003, **24**, 714–726, DOI: 10.1002/jcc.10210.
84 P. O. Dral, X. Wu, L. Sporkel, A. Koslowski, W. Weber, R. Steiger, M. Scholten and W. Thiel, *J. Chem. Theory Comput.*, 2016, **12**, 1082–1096, DOI: 10.1021/acs.jctc.5b01046.
85 D. Tuna, Y. Lu, A. Koslowski and W. Thiel, *J. Chem. Theory Comput.*, 2016, **12**, 4400–4422, DOI: 10.1021/acs.jctc.6b00403.
86 T. Shiozaki, W. Gyorffy, P. Celani and H. J. Werner, *J. Chem. Phys.*, 2011, **135**, 081106, DOI: 10.1063/1.3633329.
87 B. O. Roos, *Adv. Chem. Phys.*, 1987, **69**, 399–445, DOI: 10.1002/9780470142943.ch7.
88 J. W. Park and T. Shiozaki, *J. Chem. Theory Comput.*, 2017, **13**, 2561–2570, DOI: 10.1021/acs.jctc.7b00018.
89 S. Sen and I. Schapiro, *Mol. Phys.*, 2018, **116**, 2571–2582, DOI: 10.1080/00268976.2018.1501112.
90 I. Dokukina, C. M. Marian and O. Weingart, *Photochem. Photobiol.*, 2017, **93**, 1345–1355, DOI: 10.1111/php.12833.
91 J. Zheng, K. Kwak, X. Chen, J. B. Asbury and M. D. Fayer, *J. Am. Chem. Soc.*, 2006, **128**, 2977–2987, DOI: 10.1021/ja0570584.
92 J. Zheng and M. D. Fayer, *J. Am. Chem. Soc.*, 2007, **129**, 4328–4335, DOI: 10.1021/ja067760f.
93 D. C. Todd, J. M. Jean, S. J. Rosenthal, A. J. Ruggiero, D. Yang and G. R. Fleming, *J. Chem. Phys.*, 1990, **93**, 8658–8668, DOI: 10.1063/1.459252.
94 X. He and J. Liu, *J. Chem. Phys.*, 2019, **151**, 024105, DOI: 10.1063/1.5108736.
95 J. Liu, X. He and B. Wu, *Acc. Chem. Res.*, 2021, **54**, 4215–4228, DOI: 10.1021/acs.accounts.1c00511.
96 X. He, B. Wu, Y. Shang, B. Li, X. Cheng and J. Liu, *Wiley Interdiscip. Rev.: Comput. Mol. Sci.*, 2022, **12**, e1619, DOI: 10.1002/wcms.1619.
97 Y. Zhao and D. G. Truhlar, *Theor. Chem. Acc.*, 2008, **120**, 215–241, DOI: 10.1007/s00214-007-0310-x.
98 F. Weigend and R. Ahlrichs, *Phys. Chem. Chem. Phys.*, 2005, **7**, 3297–3305, DOI: 10.1039/b508541a.
99 M. J. Frisch, G. W. Trucks, H. B. Schlegel, G. E. Scuseria, M. A. Robb, J. R. Cheeseman, G. Scalmani, V. Barone, G. A. Petersson, H. Nakatsuji, X. Li, M. Caricato, A. V. Marenich, J. Bloino, B. G. Janesko, R. Gomperts, B. Mennucci, H. P. Hratchian, J. V. Ortiz, A. F. Izmaylov, J. L. Sonnenberg, D. Williams-Young, F. Ding, F. Lipparini, F. Egidi, J. Goings, B. Peng, A. Petrone, T. Henderson, D. Ranasinghe, V. G. Zakrzewski, J. Gao, N. Rega, G. Zheng, W. Liang, M. Hada, M. Ehara, K. Toyota, R. Fukuda, J. Hasegawa, M. Ishida, T. Nakajima, Y. Honda, O. Kitao, H. Nakai, T. Vreven, K. Throssell, J. A. Montgomery, Jr., J. E. Peralta, F. Ogliaro, M. J. Bearpark, J. J. Heyd, E. N. Brothers, K. N. Kudin, V. N. Staroverov, T. A. Keith, R. Kobayashi, J. Normand, K. Raghavachari, A. P. Rendell, J. C. Burant, S. S. Iyengar, J. Tomasi, M. Cossi, J. M. Millam, M. Klene, C. Adamo, R. Cammi, J. W. Ochterski, R. L. Martin, K. Morokuma, O. Farkas, J. B. Foresman and D. J. Fox, *Gaussian 16, Revision A.03*, Gaussian, Inc., Wallingford CT, 2016.
100 S. Kanchanakungwankul, J. Zheng, I. M. Alecu, B. J. Lynch, Y. Zhao and D. G. Truhlar, Database of Frequency Scale Factors for Electronic Model Chemistries. https://comp.chem.umn.edu/freqscale/index.html.
101 I. M. Alecu, J. J. Zheng, Y. Zhao and D. G. Truhlar, *J. Chem. Theory Comput.*, 2010, **6**, 2872–2887, DOI: 10.1021/ct100326h.
102 H. Yu, J. Zheng and D. G. Truhlar, unpublished.
103 MNDO2020 is a semiempirical quantum chemistry program written by W. Thiel, with contributions from M. Beck, S. Billeter, R. Kevorkiants, M. Kolb, A. Koslowski, S. Patchkovskii, A. Turner, E.-U. Wallenborn, and W. Weber.
104 BAGEL, Brilliantly Advanced General Electronic-structure Library. http://www.nubakery.org under the GNU General Public License.
105 T. Shiozaki, *Wiley Interdiscip. Rev.: Comput. Mol. Sci.*, 2018, **8**, e1331, DOI: 10.1002/wcms.1331.
106 T. H. Dunning, *J. Chem. Phys.*, 1989, **90**, 1007–1023, DOI: 10.1063/1.456153.